The Journal of Experimental Biology 207, 4269-4281
Published by The Company of Biologists 2004
doi:10.1242/jeb.01266

The effect of advance ratio on the aerodynamics of revolving wings

William B. Dickson* and Michael H. Dickinson
California Institute of Technology, Mail Code 138-78, Pasadena, CA 91125, USA
*Author for correspondence (e-mail: wbd@caltech.edu)

Accepted 27 August 2004

Summary

Recent studies have demonstrated that a quasi-steady model closely matches the instantaneous force produced by an insect wing during hovering flight. It is not clear, however, if such methods extend to forward flight. In this study we use a dynamically scaled robotic model of the fruit fly *Drosophila melanogaster* to investigate the forces produced by a wing revolving at constant angular velocity while simultaneously translating at velocities appropriate for forward flight. Because the forward and angular velocities were constant wing inertia was negligible, and the measured forces can be attributed to fluid dynamic phenomena. The combined forward and revolving motions of the wing produce a time-dependent free-stream velocity profile, which suggests that added mass forces make a contribution to the measured forces. We find that the forces due added mass make a small, but measurable, component of the total force and are in excellent agreement with theoretical values. Lift and drag coefficients are calculated from the force traces after subtracting the contributions due to added mass. The lift and drag coefficients, for fixed angle of attack, are not constant for non-zero advance ratios, but rather vary in magnitude throughout the stroke. This observation implies that modifications of the quasi-steady model are required in order to predict accurately the instantaneous forces produced during forward flight. We show that the dependence of the lift and drag coefficients upon advance ratio and stroke position can be characterized effectively in terms of the tip velocity ratio – the ratio of the chordwise components of flow velocity at the wing tip due to translation and revolution. On this basis we develop a modified quasi-steady model that can account for the varying magnitudes of the lift and drag coefficients. Our model may also resolve discrepancies in past measurements of wing performance based on translational and revolving motion.

Key words: flapping flight, quasi-steady force, unsteady aerodynamics, insect flight, Reynolds number, insect aerodynamics.

Introduction

Many insects are capable of performing a wide variety of sophisticated aerial maneuvers including both sustained hovering and steady forward flight. In recent years a great deal of progress has been made in our understanding of the unsteady mechanisms underlying force production during hovering flight. Evidence suggests that insects can use a variety of mechanisms, including dynamic stall (Dickinson and Gotz, 1993; Ellington et al., 1996; Sane and Dickinson, 2001), rotational lift (Bennett, 1970; Dickinson et al., 1999), wake capture (Dickinson et al., 1999; Birch and Dickinson, 2003), and the clap and fling (Weis-Fogh, 1973; Somps and Luttges, 1985; Spedding and Maxworthy, 1986). Most of these phenomena have been investigated within the context of hovering and it is not known to what extent forward velocity modifies the efficacy of these mechanisms.

Robotic models have proved a powerful tool in the investigation of aerodynamic mechanisms during flapping flight (Bennett, 1970; Maxworthy, 1979; Dickinson and Gotz, 1993; Dickinson et al., 1999; Ellington et al., 1996; Sane and Dickinson, 2001). Such models have allowed investigators to examine the effects of wing rotation as well as wing–wake and wing–wing interactions. A complication encountered when studying flapping flight using robotic models is that of isolating and quantifying the effect of a particular variable, such as wing rotation or forward velocity, upon force production. One technique commonly used by researchers to circumvent such complications is to employ extremely simplified sets of wing kinematics in order to elucidate and characterize a particular feature of force production. An example of the effective use of such a simplified set of kinematics is the study of 'revolving' wings (Usherwood and Ellington, 2002a,b) in which a propeller arrangement is used to isolate the force generation mechanisms of the downstroke and upstroke from the complicating effects of pronation and supination.

The effect of advance ratio on revolving wings has been considered previously in the context of helicopter aerodynamics (Isaacs, 1946; van der Wall and Leishman, 1994). It is difficult, however, to apply these directly to insect flight because helicopters use high aspect ratio wings operating at relatively low angles of attack, conditions atypical of insect

flight. As a result, they are more amenable to a blade element model in which sectional force coefficients derived from two-dimensional (2D) studies are used to predict total aerodynamic forces. In contrast, insect wings have a low aspect ratio, approximately 2–10 (Dudley, 2000), and typically operate at high angles of attack, often greater than 40°. Low aspect ratio wings revolving at high angles of attack are known to form a stable leading-edge vortex that is responsible for elevated force coefficients (Ellington et al., 1996; Dickinson et al., 1999; Birch and Dickinson, 2001). For this reason, previous models of insect flight have used mean sectional force coefficients derived from three-dimensional (3D) studies employing a revolving wing. These differences between the aerodynamics of helicopter rotors and insect wings highlight the need for a rigorous study of the effect of advance ratio on the forces produced by revolving wings of a shape, speed and angle of attack typical of insects.

In this study, we characterize the effect of advance ratio on aerodynamic force generation during forward flight using a dynamically scaled mechanical model of *Drosophila melanogaster*. Forces are measured over a range of advance ratios spanning the transition from hovering to fast forward flight. The kinematic pattern we used consists of a wing revolving in a horizontal stroke plane with constant angular velocity at a fixed angle of attack. From the instantaneous force records we estimate the contribution due to added mass and compare it with theoretical predictions. The added mass component is then subtracted from the force traces and mean sectional lift and drag coefficients are calculated. The mean sectional lift and drag coefficients are found to depend upon the angle of attack and the velocity profile experienced by the wing. We show that this dependence upon angle attack follows the same trigonometric relationships as that of hovering flight. However, the variation of the force coefficients with velocity profile is new and implies that modifications to the quasi-steady model are required in order to accurately predict forces during forward flight. We show that the variation of the force coefficients with velocity profile can be effectively characterized in terms of the tip velocity ratio of the wing. A modified version of the quasi-steady model is presented that incorporates this variation.

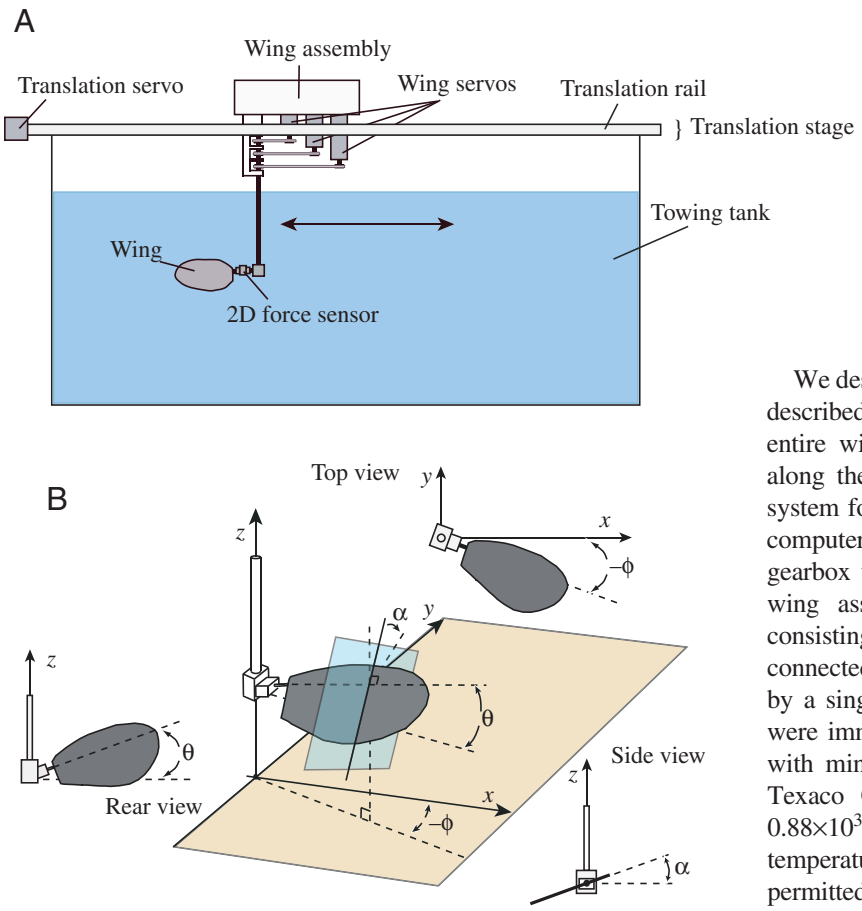

Fig. 1. (A) Diagram of robotic apparatus. The wing assembly is shown mounted on linear translation rails above the 1 m×2.4 m×1.2 m towing tank. (B) Coordinate system for the mechanical wing. Three angles are used to specify the position of the wing: ϕ, θ and α. The instantaneous stroke position, $\phi(t)$, is defined as the angular position of the projection of the wing axis in the stroke plane. The instantaneous stroke deviation, $\theta(t)$, is defined as the angle between the wing axis and the stroke plane. The instantaneous angle of attack, $\alpha(t)$, is defined as the angle between the wing's chord and the tangent to its trajectory.

Materials and methods

Robotic fly apparatus

We designed a flapping robotic apparatus, similar to that described previously (Dickinson et al., 1999), in which the entire wing assembly was capable of linear translation along the length of a towing tank (Fig. 1A). The drive system for the two wings consisted of an assembly of six computer-controlled servo-motors connected to the wing gearbox using timing belts and coaxial drive shafts. The wing assembly was mounted on a translation stage consisting of two custom linear translation rails that were connected *via* an idler bar. The translation stage was driven by a single computer-controlled servo-motor. The wings were immersed in a 1 m×2.4 m×1.2 m towing tank filled with mineral oil (Chevron Superla® white oil; Chevron Texaco Corp., San Ramon, CA, USA) of density ρ 0.88×10^3 kg m^{-3} and kinematic viscosity 115 cSt at room temperature. Custom software written in Matlab and C permitted control of the robotic model from a PC. A 2D force transducer attached to the proximal end of the wing measured forces normal and parallel to the wing surface. Each channel of the force transducer consisted of two parallel phosphor-bronze shims equipped with four 350 Ω strain gauges wired in a full-bridge configuration. We designed the force transducer to be insensitive to the position of the force load on the wing, and varying the location of the load on the wing resulted in less than 5% variation in the measured forces. The isometrically

enlarged wings of the robotic model were based on the planform of a *D. melanogaster* wing. The wings of the robotic model, cut from an acrylic sheet, had the following physical dimensions: length (R)=0.25 m, aspect ratio ($\mathcal{A}R$)=0.42, mean chord ($\bar{c}$)=0.06 m, area (S)=0.0150 m^2 and width=0.0023 m. The non-dimensional first and second moments of area of the wing are $\hat{r}_1^1(S)$=0.59 and $\hat{r}_2^2(S)$=0.39, respectively (Ellington, 1984b). In this study only a single wing of the robotic model was utilized, so the results are not influenced by wing–wing interactions.

Kinematics

In a manner similar to that described previously (Sane and Dickinson, 2001), the kinematics of the wings are specified by the time course of three angles: stroke position ϕ, the angle of attack α and stroke deviation θ (Fig. 1B). The relatively simple kinematic patterns used in this study were chosen to isolate the effects of advance ratio, stroke position, and angle of attack upon aerodynamic force generation without the additional complications of rotational forces or wing–wake interactions.

In the first set of kinematic patterns the wing was towed through the oil at constant forward velocity while at the same time revolving through a 500° arc at a constant angular velocity of ±72 deg. s^{-1}. During each trial we maintained the angle of attack at a fixed value. Four forward velocities were used in these experiments: 0, 0.04, 0.08, 0.12 and 0.16 m s^{-1}. For each forward velocity the angle of attack was systematically varied in 10° increments, from 110° to –10° for a total of 96 runs. For all of these trials, stroke deviation angle was fixed at zero. Angle of attack is defined as the angle between the wing's chord and the tangent of the wing's trajectory.

In the second set of kinematic patterns the wing was towed through the oil at constant forward velocity of 0.16 m s^{-1} at a fixed stroke position angle of 0°. During each trial we maintained the angle of attack at fixed value, which was varied from –10° to 110° in 10° increments.

Dynamic scaling

Two non-dimensional parameters are required in order to achieve an accurate dynamic scaling of the forces obtained *via* the robotic model: the Reynolds number (Re), and the advance ratio (Spedding, 1993). The Reynolds number is given by:

$$Re = \frac{R|\dot{\phi}|\bar{c}}{\nu}\,, \tag{1}$$

and the advance ratio J is given by:

$$J = \frac{V_f}{R|\dot{\phi}|}\,, \tag{2}$$

where V_f is the forward velocity and ν is the kinematic viscosity of the fluid. All of the wing kinematics used in this study were performed at Re approx. 140, matching the value appropriate for *D. melanogaster* (Lehmann and Dickinson, 1997). The advance ratios considered in this study are: ± 0, 1/8, 1/4, 3/8 and 1/2, corresponding to forward flight velocities of 0, 0.41, 0.82, 1.23 and 1.64 m s^{-1} for a fruit fly. A review of available data on *D. hydei* (David, 1978) as well as personal observations of *D. melanogaster* flying in a low-speed wind tunnel suggests that this choice of forward flight velocities spans a range from hovering to the fastest forward flight.

A third dimensionless parameter that will prove useful in our analysis is the tip velocity ratio μ:

$$\mu = \frac{V_f \cos(\phi)}{R\dot{\phi}}\,, \tag{3}$$

which is defined as the ratio of the chordwise components of flow velocity at the wing tip due to translation and revolution. Over one period of wing revolution μ will range from $-J$ to J and can be uniquely identified with a given velocity profile experienced by the wing.

Data acquisition and analysis

Force data from the 2D strain gauges were sampled at 1500 Hz using a Measurement Computing PCI-DAS-1000 Multifunction Analog digital I/O board (Middleboro, MA, USA) and filtered offline using a zero phase delay low-pass 4-pole digital Butterworth filter, with a cut-off frequency of 3 Hz. The positions of the four servo-motors were acquired simultaneously using the multifunction card and custom electronics for decoding the quadrature encoders of the servo-motors. In this manner it was possible to determine the instantaneous position of the motors, and thus the wing.

Because the stroke amplitude of most insects is less than 180° the condition when ϕ is between –90° and 90° is of particular interest. With this in mind, the stroke length used in this study was selected to meet two criteria. First, the strokes needed to be long enough so that there was sufficient time for the force transients resulting from the acceleration of the wing to disappear before ϕ was within the region –90° to 90°. Second, the strokes needed to be short enough so as not to incur any wing–wake interactions in this region. Accordingly, we chose a pattern in which the wing revolved from 250° to –250° or from –250° to 250°.

The force measured by the strain gauges at the base of the wing can be decomposed into gravitational, inertial and fluid dynamic components. The gravitational component of the measured forces is due to the mass of the wing and the mass of the sensor, and may be calculated and subtracted from the measured forces. In practice the subtraction was determined by moving the wing through sample kinematic patterns at very low velocity, for which the aerodynamic and inertial forces are negligible, and fitting the functions for the parallel and normal measured forces:

$$G_{\parallel}(\alpha) = A_{\parallel}\cos(\pi/2–\alpha) + B_{\parallel} \tag{4}$$

and

$$G_{\perp}(\alpha) = A_{\perp}\sin(\pi/2–\alpha) + B_{\perp}\,. \tag{5}$$

The functions were used to compute the gravitational forces experienced by the wing for each kinematic pattern, which were then subtracted from the measured force records.

The inertial component of the measured forces consists of two components: the action of the acceleration forces on the

mass of the wing and sensor, and the added mass of the fluid around the wing (see equation 21). The contribution of the acceleration forces of the wing and sensor masses to the total measured forces for the robotic apparatus are negligibly small (Sane and Dickinson, 2001). The added mass component experienced by the wing was estimated from the data obtained when ϕ was between –90° and 90° in the following manner. The force produced by the wing consists of the sum of the translational and added mass force components. The translational force component is typically proportional to the square of the flow velocity. Because the flow velocity is a symmetric function of stroke position, the translational force component $\mathbf{F}_t$ should also be a symmetric function, and thus $\mathbf{F}_t(\phi)$ should be equal to $\mathbf{F}_t(-\phi)$ for equal angles of attack. The added mass force is proportional to the acceleration of the flow in the direction normal to the surface of the wing. As the acceleration of the flow is an antisymmetric function of stroke position, the added mass force component $\mathbf{F}_a$ should be an antisymmetric function of stroke position, and thus $\mathbf{F}_a(\phi)$ should be equal to $-\mathbf{F}_a(-\phi)$ for equal angles of attack. This observation shows that the difference between the force measurements at stroke positions ϕ and $-\phi$ can be attributed solely to added mass component of the forces because the translational force components cancel. Thus, for fixed angle of attack the added mass force can be estimated by:

$$\mathbf{F}_a(\phi) = \tfrac{1}{2}[F(\phi)-F(-\phi)] , \quad (6)$$

where $F(\phi)$ and $F(-\phi)$ are the force measurements normal to the wing at stroke positions ϕ and $-\phi$, respectively.

The translational component of the forces was isolated by subtracting the estimates of the forces due to added mass from the measured forces. The instantaneous mean force coefficients for lift and drag were then calculated using:

$$C_L = \frac{2F_L}{\rho S(R\dot{\phi})^2[\hat{r}_2^2(S)+2\hat{r}_1^1(S)\mu+\mu^2]} , \quad (7)$$

and

$$C_D = \frac{2F_D}{\rho S(R\dot{\phi})^2[\hat{r}_2^2(S)+2\hat{r}_1^1(S)\mu+\mu^2]} , \quad (8)$$

where F_L is the measured lift, F_D is the measured drag, $\hat{r}_1^1(S)$ is the non-dimensional first moment of wing area and $\hat{r}_2^2(S)$ is the non-dimensional second moment of wing area.

Equations 7 and 8 were derived from blade element theory and take into account the changing instantaneous velocity profile experienced by the wing. When μ is equal to zero the usual mean force coefficients used for a stationary revolving wing (Osborne, 1951; Sane and Dickinson, 2001; Usherwood and Ellington, 2002a) are obtained:

$$C_L = \frac{2F_L}{\rho S(R\dot{\phi})^2\hat{r}_2^2(S)} , \quad (9)$$

and

$$C_D = \frac{2F_D}{\rho S(R\dot{\phi})^2\hat{r}_2^2(S)} . \quad (10)$$

In the limit that μ approaches infinity, equations 7 and 8 become typical mean force coefficients used in wind tunnel studies:

$$C_L = \frac{2F_L}{\rho S V_f^2 \cos^2\phi} , \quad (11)$$

and

$$C_D = \frac{2F_D}{\rho S V_f^2 \cos^2\phi} . \quad (12)$$

The force coefficients given in equations 7 and 8 can be viewed as functions of two parameters: the angle of attack α and the tip velocity ratio μ. The variation of the lift and drag coefficients with angle of attack for hovering flight is known to be well approximated by trigonometric expressions (Dickinson et al., 1999). In order to determine if these relationships are still approximately true, normalized lift and drag coefficients were derived for each angle of attack α. The normalized lift coefficient is defined by:

$$C_{L,norm}(\alpha) = \frac{C_L(\alpha,\mu)}{\max_\mu\{C_L(\alpha,\mu)\}} , \quad (13)$$

and the normalized drag coefficient is defined by:

$$C_{D,norm}(\alpha) = \frac{C_D(\alpha,\mu)-\min_\mu\{C_D(\alpha,\mu)\}}{\max_\mu\{C_D(\alpha,\mu)\}-\min_\mu\{C_D(\alpha,\mu)\}} , \quad (14)$$

where $\max_\mu$ and $\min_\mu$ are the maximum and minimum, respectively, for the given α over all μ for which there is a measurement.

In order to examine behavior of the lift and drag coefficients as a function of tip velocity ratio, μ, the measured lift and drag coefficients were fit *via* least squares, for each μ, to the following equations:

$$C_L(\alpha,\mu) = K_0(\mu)\sin\alpha\cos\alpha \quad (15)$$

and

$$C_D(\alpha,\mu) = K_1(\mu)\sin^2(\alpha)+K_2(\mu) , \quad (16)$$

where $K_0(\mu)$ is drag coefficient amplitude function, $K_1(\mu)$ is lift coefficient amplitude function, and $K_2(\mu)$ is drag coefficient offset function. Provided that for each μ the lift and drag coefficients approximately follow the trigonometric relationships with respect to α, the variation of the lift and drag coefficients will be effectively captured by the variation of $K_0(\mu)$, $K_1(\mu)$ and $K_2(\mu)$. The expressions for lift and drag coefficient given in equations 15 and 16 are periodic functions of α. The amplitude of the periodic relationships are given by $K_0(\mu)/2$ and $K_1(\mu)$, respectively, and these functions will be referred to as amplitude functions. The second term in the drag coefficient expression, $K_2(\mu)$, gives the offset of the periodic relationship from zero and is referred to as the offset function.

Quasi-steady model

In this section we extend the quasi-steady model for hovering flight (Sane and Dickinson, 2001, 2002) to the special case of forward flight consisting of a revolving wing

translating at constant forward velocity. For simplicity we assume that the angle of attack α, the angular velocity of the wing , and the forward velocity V_f, of the wing are all constant. Further, we set the deviation angle θ to zero so that the stroke plane is horizontal. In our model the instantaneous force generated by the wing is represented by the vector sum of two components:

$$\mathbf{F} = \mathbf{F}_a + \mathbf{F}_t , \tag{17}$$

where $\mathbf{F}_a$ is the force due to the added mass of the fluid and $\mathbf{F}_t$ is the instantaneous translational force.

For a wing revolving at instantaneous angular velocity and moving forward at velocity V_f, the magnitude of the sectional flow velocity is given by:

$$\dot{V}(r) = |r \quad + V_f \cos\phi| , \tag{18}$$

where r is the spanwise location of the wing section (Fig. 2). The instantaneous acceleration of the flow is the same for each wing section, i.e. it is independent of the spanwise location r, and is given by:

$$\dot{V}(r) = -V_f | \ | \sin\phi . \tag{19}$$

For an infinitesimally thin wing the existence of an acceleration in the flow implies that there will be an added mass component to the force experienced by the wing that will be proportional to the acceleration of the flow in the direction normal to the surface of the wing:

$$\dot{V}(r) \sin\alpha = -V_f | \ | \sin\phi \sin\alpha . \tag{20}$$

The magnitude of the added mass force used in this model is based on an approximation derived for the motions of an infinitesimally thin 2D flat plate in an inviscid fluid (Sedov, 1965). In a manner similar to that described by Sane and Dickinson (2001) we adapted it to the case of a 3D wing revolving at constant angular velocity and translating with forward velocity V_f through the fluid. The magnitude of the force due to the added mass, which acts normal to the wing surface, is given by:

$$F_a = -\frac{V_f|\dot{\phi}|\sin\phi\sin\alpha\rho\pi\bar{c}^2R}{4}\int_0^1 \hat{c}(\hat{r})^2 d\hat{r} , \tag{21}$$

where $\hat{r}$ is the non-dimensional spanwise wing position and $\hat{c}(\hat{r})$ is the non-dimensional mean chord. Thus, the constant of proportionality is given by:

$$\frac{\rho\pi\bar{c}^2R}{4}\int_0^1 \hat{c}(\hat{r})^2 d\hat{r} , \tag{22}$$

and has units of mass. It is known that for identical kinematics and geometry the added mass forces scale in proportion to the other aerodynamic forces (Sane and Dickinson, 2001). Thus, provided that the Reynolds number is the same, the contribution of the added mass on the wing of the robotic model and the wing of a fly should be identical.

Under the quasi-steady assumption, the translational force term $\mathbf{F}_t$ depends solely upon the instantaneous angle of attack and velocity profile experienced by the wing. $\mathbf{F}_t$ can therefore be expressed in terms of the mean sectional force coefficients in the following manner:

$$F_L = \tfrac{1}{2}\rho S C_L R^2 \ ^2[\hat{r}_2^2(S)+2\hat{r}_1^1(S)\mu+\mu^2] \tag{23}$$

and

$$F_D = \tfrac{1}{2}\rho S C_D R^2 \ ^2[\hat{r}_2^2(S)+2\hat{r}_1^1(S)\mu+\mu^2] , \tag{24}$$

where the mean sectional force coefficients, C_L and C_D, are functions of the instantaneous angle of attack α and the instantaneous velocity profile, which is uniquely determined by the tip velocity ratio μ. An appropriate expression for the dependence of the mean sectional force coefficients upon α and μ can derived under the following assumptions. First, each wing section is considered to be an infinitesimally thin 2D flat plate. Second, the component of the force resulting from pressure differences acts normal to the surface of the plate with a magnitude proportional to the projected chord of the plate perpendicular to the direction of flow. Third, the effect of skin friction is represented by a constant additive drag force. Under these three assumptions, the mean sectional lift and drag coefficients may be written as follows:

$$C_L = \left[\frac{k_{0,2}+2k_{0,1}\mu+k_{0,0}\mu^2}{\hat{r}_2^2(S)+2\hat{r}_1^1(S)\mu+\mu^2}\right]\sin\alpha\cos\alpha \tag{25}$$

and

$$C_D = \left[\frac{k_{1,2}+2k_{1,1}\mu+k_{1,0}\mu^2}{\hat{r}_2^2(S)+2\hat{r}_1^1(S)\mu+\mu^2}\right]\sin^2\alpha + \left[\frac{k_{2,2}+2k_{2,1}\mu+k_{2,0}\mu^2}{\hat{r}_2^2(S)+2\hat{r}_1^1(S)\mu+\mu^2}\right], \tag{26}$$

where the $k_{i,j}$ are unknown constants that are determined *via* a

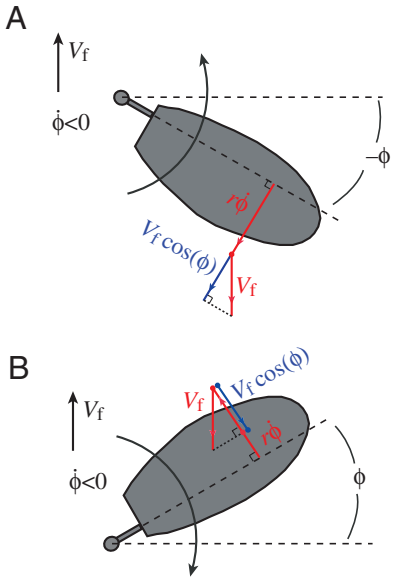

Fig. 2. Diagram of sectional flow velocities. The wing is travelling through the fluid at forward velocity V_f. (A) Downstroke. The wing is sweeping into the incident flow. The magnitude sectional flow velocity at wing position r is given by $r \ +V_f\cos(\phi)$. (B) Upstroke. The wing is sweeping with the incident flow. The flow velocity at wing position r is given by $-r \ -V_f\cos(\phi)$.

least-squares fit to a suitable data set. Detailed derivations of equations 25 and 26 are given in the Appendix.

Results

The lift and drag traces for a range of advance ratios and different angles of attack are shown in Figs 3A–D and 4A–D. Regions where the wing is between –90° and 90° roughly approximate the phase of a downstroke or an upstroke between wing rotations and are highlighted in gray. The stroke length for each experiment was selected to ensure that transient effects due to the starting accelerations had diminished to negligible levels by the time the wing was within the highlighted regions. The stroke mimics a downstroke or an upstroke when the angular velocity of the wing is equal to 72 deg. s^{-1} or –72 deg. s^{-1}, respectively.

The forces shown in Figs 3A–D, 4A–D vary with time as the wing sweeps through the background flow. Because the angular velocity of the wing is constant, the stroke position of the wing is a linear function of time. Thus, the forces in the figures may alternatively be viewed as varying with stroke position. Such a view explicitly ignores any time dependence in the flows and forces. This simplification is justified, however, because the effect of the initial stroke position did not measurably influence the ϕ-dependence of the forces. Thus, while exhibiting a dependence upon ϕ, the forces showed no intrinsic time dependence once the transients due to the starting accelerations decayed. Because the flow velocity at each wing section is a function of the stroke position, ϕ, the aerodynamic forces experienced by the wing also depend upon ϕ. During the downstroke, when the wing sweeps against the net flow, the sectional flow velocities increase from $r|\dot{\phi}|$ to $r|\dot{\phi}|+V_f$ as ϕ goes from –90° to 0°, and then decrease to $r|\dot{\phi}|$ again as ϕ goes from 0° to 90°. The lift and drag forces, which depend on the square of the flow velocity, reflect these changing velocities reaching a maximum near ϕ=0°. During the upstroke, when the wing sweeps with the background flow, the flow velocities decrease from $r|\dot{\phi}|$ to $r|\dot{\phi}|-V_f$ as ϕ goes from 90° to 0°, and increase to $r|\dot{\phi}|$ as ϕ goes from 0° to –90°. Again, the effects of the changing sectional flow velocities are reflected in the force traces. As expected, the effect of stroke position on force production is greater as advance ratio increases.

Added mass

Because the flow velocity experienced by each wing section varies with time it will experience an added mass force. This acceleration is the same for each wing section and is given by equation 19. In Fig. 5, we plot the added mass force estimated using equation 6 as a function of the absolute value of the acceleration. The theoretical estimate for the added mass force (equation 21) is shown for comparison. The magnitude of the added mass force is quite small compared to the aerodynamic forces and approaches the noise limit of our measurements for low accelerations. However, the trend is quite clear and the match between the theoretical estimate and the measured values is reasonable. The theoretical estimate of the constant of proportionality that relates acceleration to force is 0.96 kg, whereas a linear regression to the data collected in all 96 trials yields an estimated constant of proportionality of 0.98 kg, which is statistically indistinguishable from the theoretical value. This result suggests that added mass forces account for the slight asymmetry in the lift and drag forces about ϕ=0, which is evident in Figs 3 and 4.

Angle of attack

Using equations 7 and 8, lift and drag coefficients were constructed from the force traces, after subtracting the added mass component. Previous studies of hovering flight (Dickinson, 1996, 1994; Ellington and Usherwood, 2001), observed that, aside from a small contribution due to skin friction, the translational component of the force experienced by the wing is approximately normal to the surface of the wing. Fig. 6 shows a plot of force angle, the angle between the total force vector and the wing's surface, *versus* α for all 96 trials. At angles of attack above about 15° the force is approximately normal to the surface of the wing. This suggests that for high angles of attack differences in pressure normal to the surface of the wing dominate force production. For small angles of attack less than 15°, the force angle is less than 90°, an effect that can be attributed to skin friction.

Prior studies of revolving or flapping model wings (Dickinson et al., 1999; Usherwood and Ellington, 2002a,b) have shown that the mean sectional lift coefficient is proportional to $\sin(\alpha)\cos(\alpha)$, whereas the mean sectional drag coefficient, minus skin friction, is proportional to $\sin^2(\alpha)$. The quasi-steady model presented earlier in equations 25 and 26, suggests that for a fixed tip velocity ratio μ, these functional relationships will still hold. However, the constants of proportionality in the relationships are, in addition, functions of the tip velocity ratio in the case of forward flight. To test whether or not this approximation is valid, we calculated the normalized lift and drag coefficients using equations 13 and 14 (Fig. 7A,B). Plots of the functions $2\sin(\alpha)\cos(\alpha)$ and $\sin^2(\alpha)$ are shown for comparison. Agreement between the normalized coefficients and the trigonometric functions is quite close. This suggests that the mean sectional lift and drag coefficients during forward flight behave in a manner analogous to that during hovering with respect to angle of attack, provided the effects of tip velocity ratio are properly taken into account.

Tip velocity ratio

Given that the lift and drag coefficients obey the trigonometric functional relationships given by equations 15 and 16 with respect to angle of attack, the task of determining the effect of tip velocity ratio μ is reduced to characterizing the amplitude and offset functions $K_1(\mu)$, $K_2(\mu)$ and $K_3(\mu)$. In Fig. 8 we plot the drag coefficient *versus* lift coefficient for several tip velocity ratios. A fit of equations 15 and 16 for each tip velocity ratio is shown for comparison. For angles of attack greater than approximately 30°, both the lift and drag coefficients decrease with increasing tip velocity ratio. For the

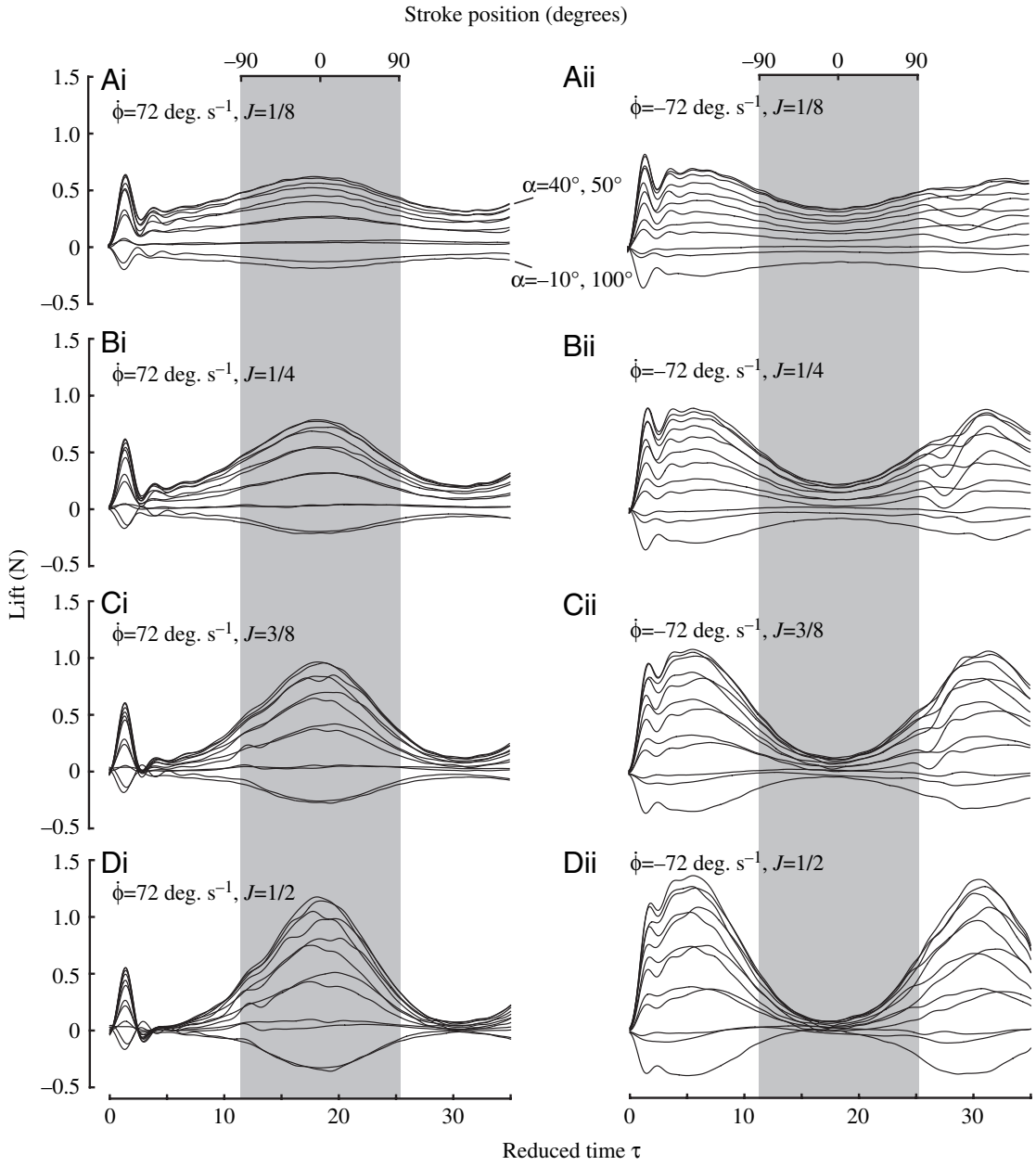

Fig. 3. Instantaneous lift traces. The regions where the stroke position of wing is between –90° and 90° are highlighted in gray and roughly approximate the phase of an upstroke, =–72 deg. s^{-1}, or downstroke, =72 deg. s^{-1}, between wing rotations. Angle of attack α is held constant in each trail and varied from –10° to 100° in steps of 10° for each advance ratio. (Ai–Di) =72 deg. s^{-1}, advance ratio equal to 1/8, 1/4, 3/8 and 1/2, respectively. (Aii–Dii) =–72 deg. s^{-1}, advance ratio equal to 1/8, 1/4, 3/8 and 1/2, respectively.

drag coefficients at small angles of attack, this trend is reversed. Also shown in Fig. 8 is a fit of equations 15 and 16 to hovering data from Birch et al. (2004). The values of the lift and drag coefficients from the hovering data coincide with the lift and drag coefficients from the zero tip velocity ratio case. In general equal tip velocity ratios, regardless of the advance ratio, result in equivalent force coefficients. However, at higher advance ratios a greater range of tip velocity ratios is achieved during each stroke.

The quasi-steady model, equations 25 and 26, suggests that an appropriate functional form for the amplitude and offset functions is that of a rational function whose numerator and denominator are second order polynomial functions of μ. The values of $K_0(\mu)$, $K_1(\mu)$ and $K_2(\mu)$ estimated from the data are shown in Fig. 9. Included in the figure for comparison are least-squares fits of the functions:

$$\frac{k_{i,2}+2k_{i,1}\,\mu+k_{i,0}\,\mu^2}{\hat{r}_2^2(S)+2\hat{r}_1^1(S)\mu+\mu^2} \tag{27}$$

to the estimated $K_1(\mu)$, $K_2(\mu)$ and $K_3(\mu)$. The agreement

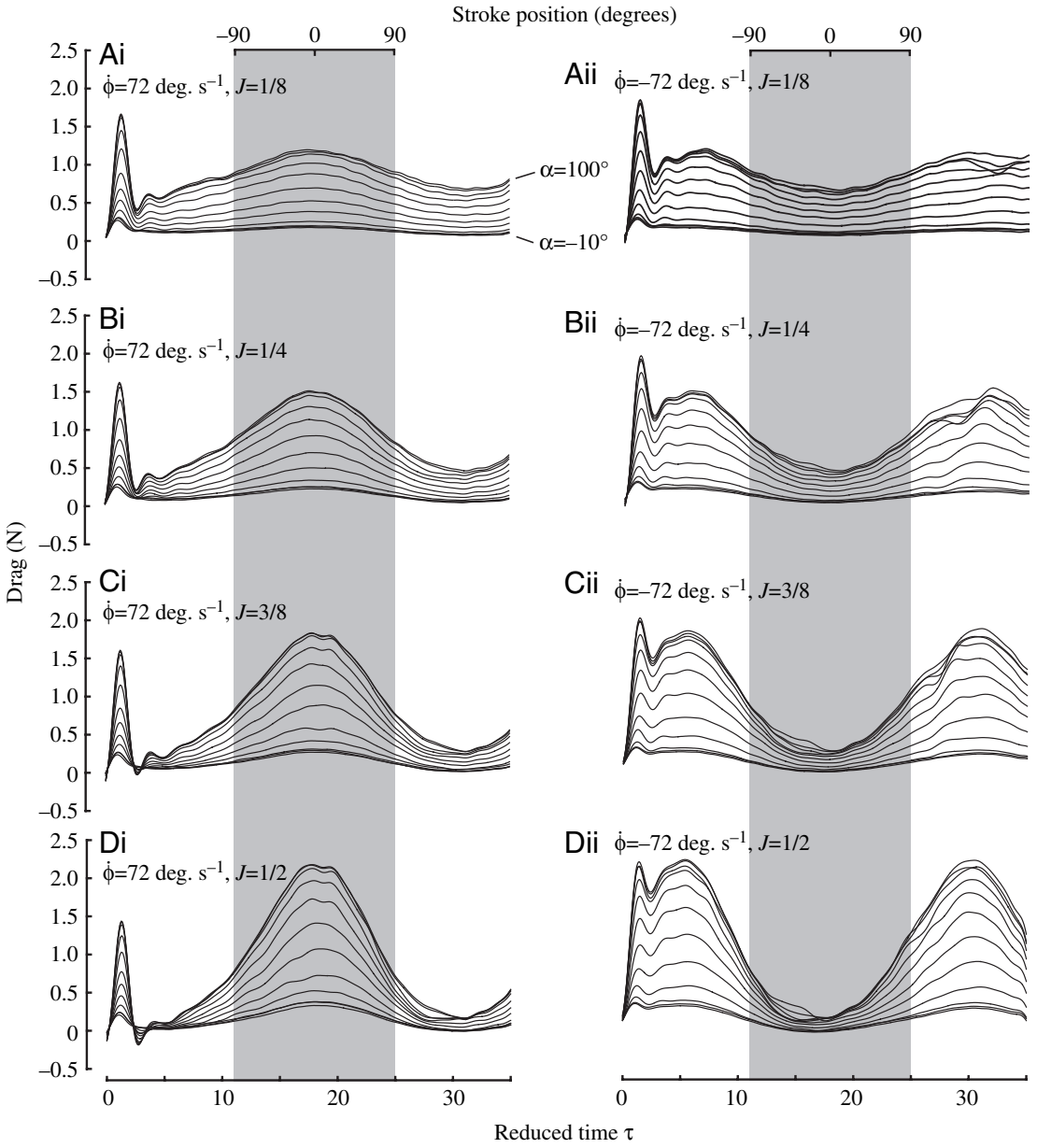

Fig. 4. Instantaneous drag traces. The regions where the stroke position of wing is between –90° and 90° are highlighted in gray and roughly approximate the phase of an upstroke or downstroke between wing rotations. Angle of attack α varied from –10° to 100° in steps of 10° for each advance ratio. (Ai–Di) =72 deg. s^{-1}, advance ratio equal to 1/8, 1/4, 3/8 and 1/2, respectively. (Aii–Dii) =–72 deg. s^{-1}, advance ratio equal to 1/8, 1/4, 3/8 and 1/2, respectively.

between the curve fits and the estimated functions is quite close, suggesting that the functional relationship provided by the model captures the behavior of the data with respect to μ remarkably well.

Fig. 10 shows a plot of the lift coefficients *versus* drag coefficients as a function of angle of attack for a non-revolving wing, with a constant forward velocity of 0.16 m s^{-1} and a fixed stroke position angle of 0°. For this set of kinematics both the advance ratio J and the tip velocity ratio μ are essentially infinite. The quasi-steady model with coefficients determined by the fit to the first set of kinematic patterns, with μ between –0.5 and 0.5, can be extrapolated to predict the lift and drag coefficients for the non-revolving wing by taking the limit of equations 25 and 26 as μ approaches infinity:

$$C_{\mathrm{L}} = k_{0,0}\sin(\alpha)\cos(\alpha)\,, \tag{28}$$

and

$$C_{\mathrm{D}} = k_{1,0}\sin^2(\alpha) + k_{2,0}\,. \tag{29}$$

Plots of equations 28 and 29 are shown in Fig. 10 for comparison. The predicted and measured coefficients agree reasonably well and the extrapolation of the quasi-steady model accurately captures the trend as μ approaches infinity.

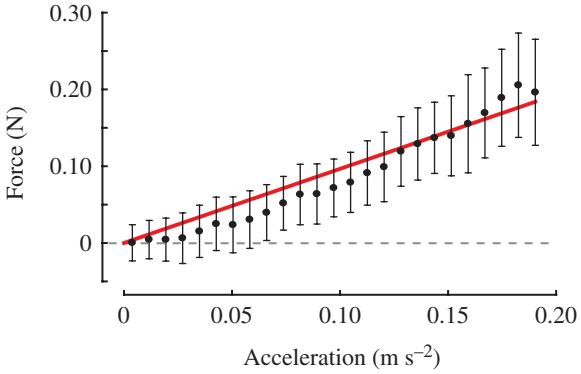

Fig. 5. Added mass component of the measured force as a function of acceleration for all 96 trials (black circles). The theoretical estimate from Sedov model is shown in red. Values are means ± 1 S.D.

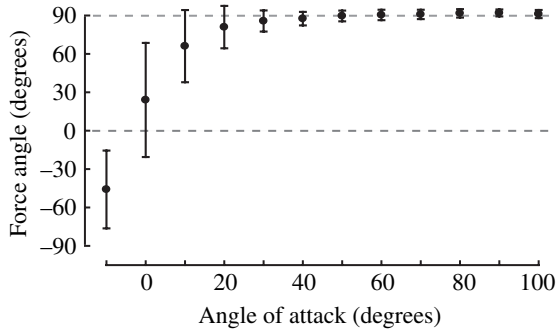

Fig. 6. Mean angle between the wing and the net force vector as a function of angle of attack. Values are means ± 1 S.D.

Discussion

We used a dynamically scaled model to measure the instantaneous lift and drag forces produced by a simultaneously revolving and translating wing. The results enable us to characterize the effect of advance ratio in the absence of rotational forces and wing–wake interactions. The force produced by the wing can be decomposed into two parts: an added mass force and a translational component. The added mass component of the force was measured using the asymmetry in the forces with respect to stroke position and closely matched theoretical predictions (Fig. 5). Lift and drag coefficients for the translational force component were constructed after subtracting the contribution due to added mass. The lift and drag coefficients follow simple trigonometric relationships with respect to angle of attack: the lift coefficient is proportional to $\sin(\alpha)\cos(\alpha)$ and the drag coefficient to $\sin^2(\alpha)$ (Fig. 7). The amplitude and offset of the these relationships is not constant, but depends upon the velocity profile experienced by the wing. As the velocity profile is completely determined by the tip velocity ratio, we demonstrated that it is possible to characterize the dependence of the force coefficients on the velocity profile in terms of the tip velocity ratio. The fact that the lift and drag coefficients depend upon the tip velocity ratio implies that modifications of the quasi-steady model are required in order accurately to predict forces during forward flight. To this end a modified quasi-steady model that is capable of incorporating the dependence of the force coefficients on the tip velocity ratio was introduced. Finally, it was shown that the modified quasi-

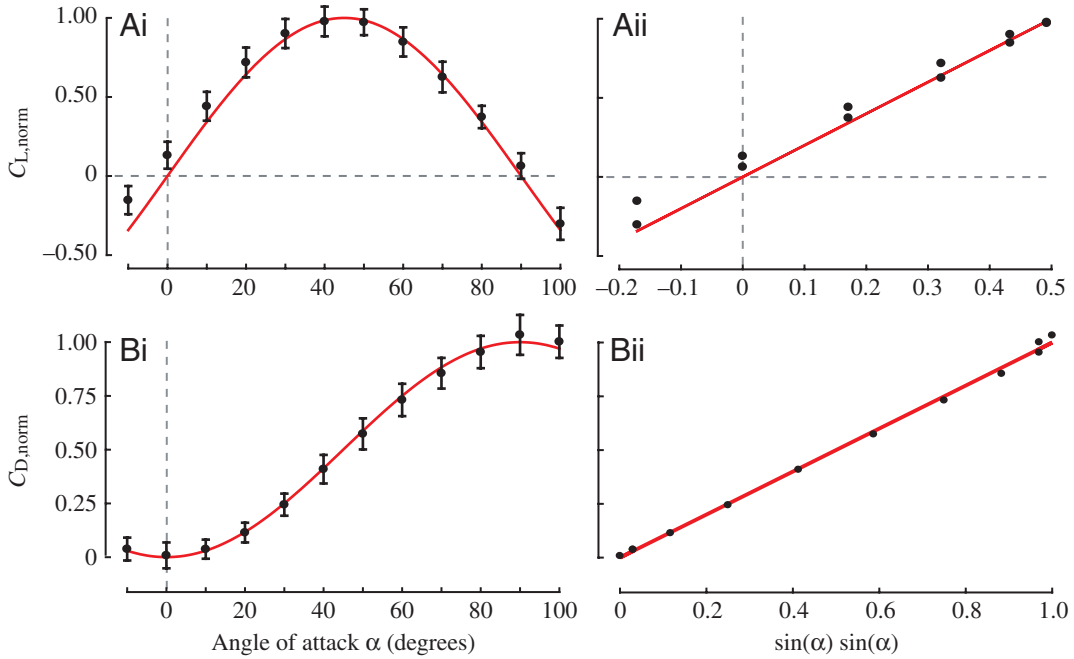

Fig. 7. Normalized lift and drag coefficients for all 96 trials. (Ai,Bi) Normalized lift and drag coefficients as a function of angle of attack, α, respectively (black circles). The functions $\sin(\alpha)\cos(\alpha)$ and $\sin(\alpha)\sin(\alpha)$ are shown for comparison (red). (Aii,Bii) Normalized lift and drag coefficients as a function of $2\sin(\alpha)\cos(\alpha)$ and $\sin(\alpha)\sin(\alpha)$, respectively. The identity function is shown for comparison in red. Normalized coefficients were computed from the data highlighted in gray in Figs 3 and 4 using equations 13 and 14. Values are means ±1 S.D.

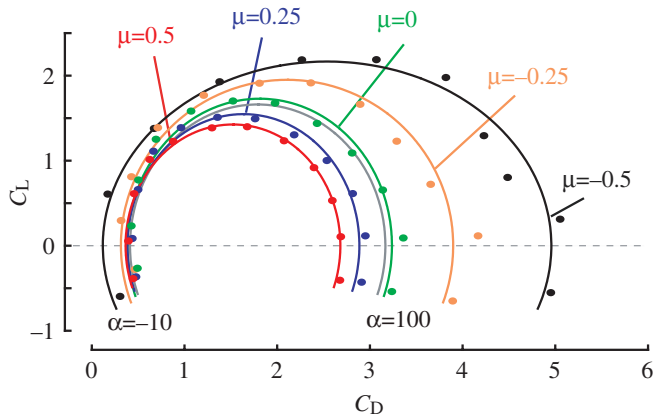

Fig. 8. Lift coefficient C_L *versus* drag coefficient C_D as a function of angle of attack for various tip velocity ratios (μ): 0.5 (red), 0.25 (blue), 0 (green), –0.25 (orange), –0.5 (black). A fit of equations 15 and 16 to hovering data is shown for comparison (gray).

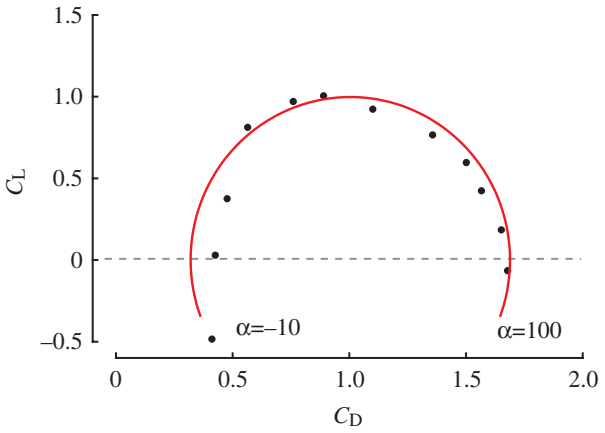

Fig. 10. Lift coefficient C_L and drag coefficient C_D as a function of angle of attack for steadily translating non-revolving wing (black circles). Predicted lift and drag coefficients from equations 25 and 26 in the limit as μ approaches infinity (red line).

steady model generalizes in the correct manner as the tip velocity ratios become large, as in the case of pure translation.

Added mass forces

The added mass forces estimated from experimental data closely agree with the theoretical predictions made using equation 21. Both the measured and predicted forces were quite small in magnitude and represent less than 10% of the total force generated by the wing. Also, over the course of an actual stroke cycle they would average to zero so that net their effect on average forces is insignificant. Nevertheless, it is possible that they remain large enough to play a role in the delicate force and moment balance that takes place during aerial maneuvers.

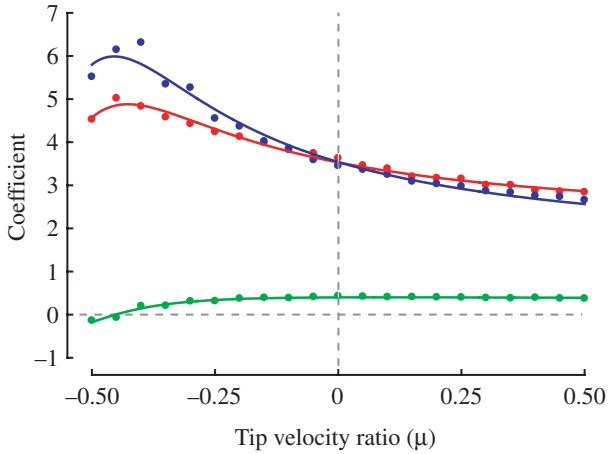

Fig. 9. Lift and drag coefficient amplitude and offset functions determined *via* least-squares fit of equations 15 and 16. Lift amplitude function $K_0(\mu)$ (blue circles), Drag amplitude function $K_1(\mu)$ (red circles), and drag offset function $K_2(\mu)$ (green circles). Fit of equation 27 to the amplitude and offset functions. Lift amplitude fit (blue line) $k_{0,2}$=1.38, $k_{0,1}$=1.65 and $k_{0,0}$=2.01. Drag amplitude fit (red line) $k_{1,2}$=1.38, $k_{1,1}$=1.44 and $k_{1,0}$=1.38. Drag offset fit (green line) $k_{2,2}$=0.15, $k_{2,1}$=0.24 and $k_{2,0}$=0.32.

For the kinematics considered in this study, the theoretical predictions of the added mass force, based on an approximation given in Sedov (1965), match the estimates from experimental data quite well. It has been shown, however, that for some types of wing kinematics this is not the case. Birch and Dickinson (2003) considered the forces produced by a back-and-forth flapping pattern in which the time course of stroke position is a filtered triangle wave. They observed that the time course of the forces generated at the start of a stroke were not well matched by the same added mass model considered here. This discrepancy held even for impulsive starts, when wing–wake interactions are not present. A significant difference between the two cases is that magnitude of the peak acceleration in the back-and-forth pattern was approximately 10 times greater than those of the revolving and translating wing in this study. Thus, it appears the Sedov model is reasonably accurate for the more gentle accelerations but underestimates forces during higher accelerations.

Translational forces

The quasi-steady model of the translational force coefficients, equations 25 and 26, is based on a blade element derivation. In this treatment, the sectional force coefficients vary with spanwise location, a dependence embodied by the functions $k_j(\hat{r})$ in equations A1 and A2. In contrast, previous work on revolving wings under hovering conditions have employed mean sectional force coefficients that are assumed constant with respect to spanwise location (Sane and Dickinson, 2001; Usherwood and Ellington, 2002a). In the zero advance ratio limit such an assumption is not detrimental, because for a given angle of attack the mean sectional force coefficients are not sensitive to variations in velocity provided that the dependence of the sectional force coefficients on span, regardless of form, does not vary over the range of velocities

considered. However, the simplification does not hold at finite advance ratio. With the addition of forward velocity, the mean force coefficients may become sensitive to variations in the flow velocity profile experienced by the wing. Even assuming that the functional dependence of the sectional force coefficients upon span remains the same, the mean force coefficients may depend upon the instantaneous velocity profile experienced by the wing. Only in the special case where the sectional coefficients are constant with respect to span does the dependence of the mean force coefficients upon the velocity profile disappear. This effect complicates the analysis of forward flight and was the reason we adopted a more general approach here. Theoretical considerations that take into account the effect of tip vortices (Katz and Plotkin, 2001) as well as recent experimental results (Birch and Dickinson, 2003) suggest that for each angle of attack the sectional force coefficients do indeed depend upon span. The exact form of this dependence, and whether for each angle of attack the sectional force coefficients are dependent or independent of the velocity profile, is not yet known.

Mean sectional force coefficients determined from zero advance ratio data as a function of angle of attack are available for various wing planforms and at various Reynolds numbers (Sane and Dickinson, 2001; Usherwood and Ellington, 2002a,b; Birch et al., 2004). For this reason it is interesting to compare the total force coefficients estimated from the forward flight data using equations 25 and 26, with those from hovering data. The force coefficients from hovering data agree with the coefficients from forward flight data when the tip velocity ratio $\mu=0$. For angles of attack typical of insect flight (30–90°) at tip velocity ratios <0, the lift and drag coefficients are greater than those during hovering flight, and at tip velocity ratios >0 the lift and drag coefficients are less than those during hovering flight. For low advance ratios (<0.1), this discrepancy can probably be ignored without incurring too much error. However, as advance ratio increases modifications are required in order to predict forces accurately.

The quasi-steady model, with coefficients derived from finite advance ratio data, was found to extrapolate fairly well to steadily translating wings (Fig. 10). The model as currently posed attributes the difference in force coefficients entirely to the effect of the instantaneous velocity profile on the constant spanwise distribution of sectional force coefficients. In particular, it is assumed that the the spanwise distribution of sectional forces coefficients for a given angle of attack does not itself depend on the velocity profile. This is probably not entirely true. However, it appears to be a reasonable approximation for tip velocity ratio between –0.5 and 0.5. It also captures the trend correctly at high advance ratios. Validation of this assumption will require measurements of the spanwise loading of a wing at various tip velocity ratios.

Interest in the possible role of unsteady effects in insect flight was stimulated in large part by the comprehensive analysis of Ellington (1984a), in which he tested the feasibility of quasi-steady models using a ‘proof by contradiction’. He compared available experimental measures of the maximum steady-state lift coefficients in the literature with the values required to support hovering flight based on body morphology and simplified wing kinematics. His conclusion was that experimental values were typically too low to account for the forces required to sustain flight, thus justifying a search for unsteady effects that might account for the elevated performance of insect wings under flapping conditions. However, the conclusions of Ellington’s thorough analysis are in conflict with recent studies demonstrating that revolving wings create constant force in the Reynolds number range used by insects (Dickinson et al., 1999; Usherwood and Ellington, 2002a). More specifically, although revolving wings separate flow and create a leading edge vortex, this flow structure is stable over many chord lengths. Given these recent results it is perplexing why Ellington’s metanalysis demonstrated an insufficiency of quasi-steady models based on previous measures of force coefficients on real and model wings in steady translating flow. The results of our analysis offer a possible explanation for this discrepancy. Namely, that the maximum steady-state lift coefficient depends upon the velocity profile experienced by the wing, and use of lift coefficients from steadily translating wings, with essentially infinite tip velocity ratio, leads to an underestimate of the possible lift for a flapping or revolving wing. From these results it is clear that unsteady mechanisms may not be required in order to explain the force balance for a hovering insect, but only that the appropriate force coefficients be used.

Implications of kinematics

During steady forward flight it is likely that an insect must adopt appropriate wing kinematics to balance lift, thrust and body moments at each forward velocity. Several studies (David, 1978; Willmott and Ellington, 1997) that have examined the relationship between forward flight speed and body angle found an inverse correlation, such that the angle between the insects body and the horizontal plane decreases with increasing flight speed. Further, in a study of *Manduca sexta*, Willmott and Ellington (1997) demonstrated that there is a positive correlation between stroke plane angle and forward speed. During forward flight the angle of attack, and thus the instantaneous forces produced, depend strongly upon the stroke plane angle. From these studies it is clear that wing kinematics, at least *via* changes in stroke plane angle, do indeed vary in a systematic manner with forward velocity. Without a comprehensive understanding of force production for arbitrary wing kinematics over a suitable range of advance ratios it is difficult to interpret how the observed changes in wing motion effect the appropriate force and moment balance.

In order to keep things as simple as possible the kinematics employed in this study all had a stroke plane angle of zero, which we know to be unrealistic. It is not yet known how changes in stroke plane angle will further modify the measured

lift and drag coefficients. Further studies are required to determine the combined effect of forward velocity and nonzero stroke plane angles.

Appendix

An appropriate functional representation of the mean sectional lift and drag coefficients can be derived as follows. First, each wing section is considered to be an infinitesimally thin 2D flat plate. Second, the component of the force resulting from pressure differences acts normal to the surface of the plate with a magnitude proportional to the projected chord of the plate perpendicular to the direction of flow. Third, the effect of skin friction is represented by a constant additive drag force. Under these three assumptions, the sectional force coefficients may be written as:

$$C'_{\mathrm{L}}(\hat{r}) = k_0(\hat{r})\sin(\alpha)\cos(\alpha)\,, \tag{A1}$$

and

$$C'_{\mathrm{D}}(\hat{r}) = k_1(\hat{r})\sin^2(\alpha) + k_2(\hat{r})\,, \tag{A2}$$

where the functions $k_1(\hat{r})$, $k_2(\hat{r})$ and $k_3(\hat{r})$ describe the dependence on the spanwise location of the wing section. The sectional lift and drag forces as a function of non-dimensional spanwise location of the wing section are then given by:

$$F'_{\mathrm{L}}(\hat{r}) = \tfrac{1}{2}\rho c(\hat{r})C_{\mathrm{L}}(\hat{r})[\hat{r}R\ + V_{\mathrm{f}}\cos(\phi)]^2\,, \tag{A3}$$

and

$$F'_{\mathrm{D}}(\hat{r}) = \tfrac{1}{2}\rho c(\hat{r})C_{\mathrm{D}}(\hat{r})[\hat{r}R\ + V_{\mathrm{f}}\cos(\phi)]^2\,. \tag{A4}$$

Integrating the sectional lift and drag forces along the span of the wing and substituting equations A1 and A2 for the sectional lift and drag coefficients yields the following expressions for the magnitudes of the total lift and drag forces experienced by the wing:

$$F_{\mathrm{L}} = \tfrac{1}{2}\rho SR^2\ \ ^2(k_{0,2}+2k_{0,1}\mu+k_{0,0}\mu^2)\sin(\alpha)\cos(\alpha)\,, \tag{A5}$$

and

$$F_{\mathrm{D}} = \tfrac{1}{2}\rho SR^2\ \ ^2[(k_{1,2}+2k_{1,1}\mu+k_{1,0}\mu^2)\sin^2(\alpha) + (k_{2,2}+2k_{2,1}\mu+k_{2,0}\mu^2)]\,, \tag{A6}$$

where

$$k_{\mathrm{i,j}} = \int_0^1 \hat{r}^{\mathrm{j}}k_{\mathrm{i}}(\hat{r})\hat{c}(\hat{r})\mathrm{d}\hat{r}\,. \tag{A7}$$

Equating the expressions for lift and drag given by equations 23 and 24 and by equations A5 and A6, respectively, and then solving for the lift and drag coefficients, yields the desired expressions for the mean sectional lift and drag coefficients:

$$C_{\mathrm{L}} = \left[\frac{k_{0,2}+2k_{0,1}\mu+k_{0,0}\mu^2}{\hat{r}^2_2(S)+2\hat{r}^1_1(S)\mu+\mu^2}\right]\sin\alpha\cos\alpha \tag{A8}$$

and

$$C_{\mathrm{D}} = \left[\frac{k_{1,2}+2k_{1,1}\mu+k_{1,0}\mu^2}{\hat{r}^2_2(S)+2\hat{r}^1_1(S)\mu+\mu^2}\right]\sin^2\alpha + \left[\frac{k_{2,2}+2k_{2,1}\mu+k_{2,0}\mu^2}{\hat{r}^2_2(S)+2\hat{r}^1_1(S)\mu+\mu^2}\right]. \tag{A9}$$

List of symbols

$\mathcal{AR}$	aspect ratio
$A_{\parallel}$	parallel gravitational force amplitude constant
$A_{\perp}$	normal gravitational force amplitude constant
$B_{\parallel}$	parallel gravitational force offset constant
$B_{\perp}$	normal gravitational force offset constant
$c(r)$	chord length
$\hat{c}(\hat{r})$	non-dimensional chord length
$\bar{c}$	mean chord length
C_{L}	mean sectional lift coefficient
$C'_{\mathrm{L}}(\hat{r})$	sectional force coefficient
$C_{\mathrm{L,norm}}(\alpha)$	normalized lift coefficient
C_{D}	mean sectional drag coefficient
$C'_{\mathrm{D}}(\hat{r})$	sectional drag coefficient
$C_{\mathrm{D,norm}}(\alpha)$	normalized drag coefficient
$\mathbf{F}$	instantaneous aerodynamic force
$\mathbf{F}_{\mathrm{a}}$	added mass force
F_a	magnitude of added mass force
F_{D}	total drag
$F'_{\mathrm{D}}(\hat{r})$	sectional drag
F_{L}	total lift
$F'_{\mathrm{L}}(\hat{r})$	sectional lift
$\mathbf{F}_{\mathrm{t}}$	translational force
$F(\phi)$	force measurement normal to the wing at stroke position ϕ
$G_{\parallel}(\alpha)$	gravitational force parallel to wing
$G_{\perp}(\alpha)$	gravitational force parallel to wing
J	advance ratio
$k_1(\hat{r})$	sectional lift amplitude function
$k_2(\hat{r})$	sectional drag amplitude function
$k_3(\hat{r})$	sectional drag offset function
$k_{\mathrm{i,j}}$	lift and drag coefficient integrals/fit coefficients
$K_0(\mu)$	drag coefficient amplitude function
$K_1(\mu)$	lift coefficient amplitude function
$K_2(\mu)$	drag coefficient offset function
r	radial position along wing
$\hat{r}$	non-dimensional radial position along wing
$\hat{r}^1_1(S)$	non-dimensional first moment of wing area
$\hat{r}^2_2(S)$	non-dimensional second moment of wing area
R	wing length
Re	Reynolds number
S	wing area
V_{f}	forward velocity
$V(r)$	sectional flow velocity
$\alpha(t)$	instantaneous angle of attack
	angular velocity of the wing
$\phi(t)$	instantaneous stroke position
μ	tip velocity ratio
$\theta(t)$	instantaneous stroke deviation density of fluid
ν	kinematic viscosity
τ	reduced time $t\ \ \lvert R(\bar{c})^{-1}$

This work was supported by the Packard Foundation and the National Science Foundation (IBN-0217229).

References

Bennett, L. (1970). Insect flight: lift and rate of change of incidence. *Science* **167**, 177-179.

Birch, J. M. and Dickinson, M. H. (2001). Spanwise flow and the attachment of the leading-edge vortex on insect wings. *Nature* **412**, 729-733.

Birch, J. M. and Dickinson, M. H. (2003). The influence of wing–wake interactions on the production of aerodynamic forces in flapping flight. *J. Exp. Biol.* **206**, 2257-2272.

Birch, J. M., Dickson, W. B. and Dickinson, M. H. (2004). Force production and flow structure of the leading edge vortex on flapping wings at high and low Reynolds numbers. *J. Exp. Biol.* **207**, 1063-1072.

David, C. T. (1978). Relationship between body angle and flight speed in free-flying *Drosophila*. *Physiol. Ent.* **3**, 191-195.

Dickinson, M. H. (1994). The effects of wing rotation on unsteady aerodynamic performance at low Reynolds numbers. *J. Exp. Biol.* **192**, 179-206.

Dickinson, M. H. (1996). Unsteady mechanisms of force generation in aquatic and aerial locomotion. *Am. Zool.* **36**, 537-554.

Dickinson, M. H. and Gotz, K. G. (1993). Unsteady aerodynamic performance of model wings at low Reynolds numbers. *J. Exp. Biol.* **174**, 45-64.

Dickinson, M. H., Lehmann, F. O. and Sane, S. P. (1999). Wing rotation and the aerodynamic basis of insect flight. *Science* **284**, 1954-1960.

Dudley, R. (2000). *The Biomechanics of Insect Flight*. Princeton University Press, Princeton, New Jersey.

Ellington, C. P. (1984a). The aerodynamics of hovering insect flight. I lift and power requirements. *Phil. Trans. R. Soc. Lond. B* **305**, 1-15.

Ellington, C. P. (1984b). The aerodynamics of hovering insect flight. II. morphological parameters. *Phil. Trans. R. Soc. Lond. B* **305**, 17-40.

Ellington, C. P. (1984c). The aerodynamics of hovering insect flight. III. kinematics. *Phil. Trans. R. Soc. Lond. B* **305**, 41-78.

Ellington, C. P. and Usherwood, J. R. (2001). Lift and drag characteristics of rotary and flapping wings. *Progr. Aeronaut. Astronaut. AIAA* **195**, 231-248. Reston, Virginia: American Institute of Aeronautics and Astronautics, Inc.

Ellington, C. P., vandenBerg, C., Willmott, A. P. and Thomas, A. L. R. (1996). Leading-edge vortices in insect flight. *Nature* **384**, 626-630.

Isaacs, R. (1946). Airfoil theory for rotary wing aircraft. *J. Aeronaut. Sci.* **13**, 218-220.

Katz, J. and Plotkin, A. (2001). *Low-Speed Aerodynamics*. Cambridge, UK: Cambridge University Press.

Lehmann, F. O. and Dickinson, M. H. (1997). The changes in power requirements and muscle efficiency during elevated force production in the fruit fly *Drosophila melanogaster*. *J. Exp. Biol.* **200**, 1133-1143.

Maxworthy, T. (1979). Experiments on the Weis-Fogh mechanism of lift generation by insects in hovering flight. Part 1. Dynamics of the 'fling'. *J. Fluid Mech.* **93**, 47-63.

Osborne, M. F. M. (1951). Areodynamics of flapping flight with application to insects. *J. Exp. Biol.* **28**, 221-245.

Sane, S. P. and Dickinson, M. H. (2001). The control of flight force by a flapping wing: Lift and drag production. *J. Exp. Biol.* **204**, 2607-2626.

Sane, S. P. and Dickinson, M. H. (2002). The aerodynamic effects of wing rotation and a revised quasi-steady model of flapping flight. *J. Exp. Biol.* **205**, 1087-1096.

Sedov, L. I. (1965). *Two-Dimensional Problems in Hydrodynamics and Aerodynamics*. New York: Interscience Publishers.

Somps, C. and Luttges, M. (1985). Dragonfly flight – novel uses of unsteady separated flows. *Science* **228**, 1326-1329.

Spedding, G. R. (1993). On the significance of unsteady effects in the aerodynamic performance of flying animals. *Contemp. Math.* **141**, 247-272.

Spedding, G. R. and Maxworthy, T. (1986). The generation of circulation and lift in a rigid two-dimensional fling. *J. Fluid Mech.* **165**, 247-272.

Usherwood, J. R. and Ellington, C. P. (2002a). The aerodynamics of revolving wings. I. Model hawkmoth wings. *J. Exp. Biol.* **205**, 1547-1564.

Usherwood, J. R. and Ellington, C. P. (2002b). The aerodynamics of revolving wings. II. Propeller force coefficients from mayfly to quail. *J. Exp. Biol.* **205**, 1565-1576.

van der Wall, B. G. and Leishman, J. G. (1994). On the influence of time-varying flow velocity on unsteady aerodynamics. *J. Am. Heli. Soc.* **26**, 25-36.

Weis-Fogh, T. (1973). Quick estimates of flight fitness in hovering animals, including novel mechanisms for lift production. *J. Exp. Biol.* **59**, 169-230.

Willmott, A. P. and Ellington, C. P. (1997). The mechanics of flight in the hawkmoth *Manduca sexta*. I. Kinematics of hovering and forward flight. *J. Exp. Biol.* **200**, 2705-2722.